# Single-shot phase-matching free ultrashort pulse characterization based on transient absorption in solids

Benoit Brizard, Adrien Leblanc, Stephane Petit, Jean-Christop Delagnes, Éric Cormier, Heide Ibrahim, François Légaré, Philippe Lassonde

Research Article | Vol. 28, No. 24 / 23 November 2020 / Optics Express 35807
Optics EXPRESS

# Single-shot phase-matching free ultrashort pulse characterization based on transient absorption in solids

BENOIT BRIZARD,[1] ADRIEN LEBLANC,[2] STÉPHANE PETIT,[3] JEAN-CHRISTOPHE DELAGNES,[3] ÉRIC CORMIER,[4,5] HEIDE IBRAHIM,[1] FRANÇOIS LÉGARÉ,[1,6] AND PHILIPPE LASSONDE[1,7]

[1]*Institut National de la Recherche Scientifique, centre Énergie, Matériaux et Télécommunications, 1650 blvd Lionel-Boulet, Varennes J3X1S2, Canada*
[2]*Laboratoire d'Optique Appliquée, École Polytechnique, ENSTA, CNRS, Université Paris Saclay, Palaiseau, France*
[3]*Centre National de la Recherche Scientifique, Centre Lasers Intenses et Applications, 351, Cours de la Libération, Talence, France*
[4]*Laboratoire Photonique Numérique et Nanosciences (LP2N),UMR 5298, CNRS-IOGS-Université Bordeaux, 33400 Talence, France*
[5]*Institut Universitaire de France (IUF), 1 rue Descartes, 75231 Paris Cedex 05, France*
[6]*legare@emt.inrs.ca*
[7]*lassonde@emt.inrs.ca*

**Abstract:** The frequency-resolved optical switching (FROSt) method developed for ultrashort pulse characterization is implemented for single-shot measurements. In this basic demonstration, the delay axis of the spectrogram is spatially encoded by the pump beam having a small incident angle with the photoexcited material. We present the calibration procedure for spectrograms acquired in single-shot and the temporal characterization of 44 fs pulses with central wavelength at 800 nm both in scanning and single-shot FROSt configurations. The retrieved pulses are compared by means of the root-mean-square field error. Finally, the pulses are propagated through a known dispersive material to measure the added group-delay dispersion.



## 1. Introduction

After more than three decades of intensive development of ultrafast laser technologies, numerous diagnostics have been developed for characterizing femtosecond optical pulses. For a review on this vast topic, we suggest, among others, the following literature: [1,2]. While interferometric methods are more convenient for single-shot measurements because the amplitude and phase of the field are encoded in a single spectrum [3,4], most techniques have been adapted to single-shot versions, if only to avoid time-consuming acquisitions or to circumvent the problem of pulse-to-pulse fluctuations [5–9]. Nevertheless, there is still a need for reliable diagnostics specifically adapted to low repetition rate and broadband laser systems, potentially operating under vacuum [10–13]. Here, we report on the basic implementation of the single-shot frequency resolved optical switching (FROSt) technique, previously developed in our group [14], in a configuration enabling the complete characterization of ultrashort pulses in a single shot. FROSt is a phase-matching free pulse characterization technique associating transient absorption to ptychographic reconstruction for pulse retrieval. So far, it has been used in a scanning manner for the characterization of broadband pulses with central wavelength from the near-infrared to the mid-infrared, such as few-cycle pulses at 10 µm derived from an optical parametric amplifier [15]. However, for many experiments, it is crucial to obtain the pulse information in a single shot, whether it is to obtain a real-time post-treatment and feedback or to be used with low repetition

#409342 https://doi.org/10.1364/OE.409342
Journal © 2020 Received 9 Sep 2020; revised 19 Oct 2020; accepted 20 Oct 2020; published 10 Nov 2020

Optics EXPRESS

rate laser systems. For this purpose, we have adapted the FROSt technique for single-shot operation.

Briefly, an ultrashort pulse referred to as the pump is applied with sufficient fluence at the surface of a material, typically from tens to hundreds of mJ/cm$^2$, to photo-excite the sample (e.g. here ZnSe). This induces a transient switching of its transmissivity attributed to the sudden increase of the free carrier density near the surface of the material. This creates an ultrafast switch, or a temporal knife-edge for the signal to be characterized. Then, the pulse to be characterized propagates through the material and probes the ultrafast switch. Its transmitted spectrum is measured as a function of the relative delay between the two pulses. The spectral intensity and phase of the probe pulse are this way encoded in the frequency-resolved transition and can be extracted from the spectrogram with, for instance, a ptychographic phase retrieval algorithm [16]. So far, measurements have been performed in a scanning sequence where the relative delay of the switch is varied using a standard optical delay line with mirrors on a motorized translation stage. As detailed in the next section, to perform this measurement in single-shot, the variable delay is made with the pump beam having a small incident angle with the surface of the sample. Our configuration is similar to the one employed for the demonstration of the single-shot frequency-resolved optical gating (FROG) technique in this pioneering work [5]. We perform a comparative study between the single-shot and the delay-scanning FROSt configurations by characterizing pulses from a standard Ti:sapphire laser system.

## 2. Single-shot FROSt optical layout

The optical layout for single-shot FROSt measurements is illustrated in Fig. 1(a). At the sample, the relative delay is spatially encoded in the vertical direction by the pump beam having a small incidence angle θ with respect to the material surface in this direction. This way, the relative delay of the pump is changing across the vertical dimension of the sample like illustrated in Fig. 1(b). In the horizontal direction, the transmitted spectrum of the probe beam is frequency-resolved with a grating-based 2-D spectrometer. This way, a 2-D FROSt spectrogram is acquired in a single sequence with a CCD camera positioned in a plane where the vertical dimension corresponds to the delay axis, and the horizontal dimension to the spectral axis. Indeed, it is essential to calibrate these two axes prior to reconstruct the experimental spectrograms.

In this geometry, the coordinate system $xyz$ is defined from the probe beam propagation axis $z$, with transverse directions $x$, horizontal/parallel to the optical table, and $y$, vertical. This Cartesian coordinate system is illustrated in Figs. 1(a)-(d). The output pulse of the laser is divided in two arms by means of a beamsplitter (BS). The BS is used to send the probe beam towards mirrors fixed on a translation stage to finely adjust the zero delay between the two optical arms. Before reaching the sample, the pump beam is deflected in the vertical direction to create a small incident angle θ at the surface of the material. The two separated beams are focused with cylindrical lenses along lines in the $y$/vertical direction where they are superposed at the surface of a ZnSe sample as illustrated in Fig. 1(c), with the probe beam in red and the pump beam in dark red. The pump beam has sufficient fluence to create the switch at the surface of the material. This way, the switch and the probe have a relative delay changing in the vertical direction as $dt_0/dy = -\tan(\theta)/c$ with c the speed of light. In practice, like for other single-shot techniques [5,17], measuring the precise incident angle is not necessary because changing the delay by a known value can be observed directly in the measured signal (described in section 3).

After its transmission through the photoexcited material, the probe beam is frequency resolved continuously along its vertical dimension (Fig. 1(d)), and the spectrogram corresponding to the FROSt signal $I(\lambda,t_0)= |F\{P(t)*S(t-t_0)\}|^2$ is imaged on a CCD camera, with $P(t)$ and $S(t)$ being the complex probe and switch functions, respectively. This way, the signal $I(\lambda,t_0)$ is acquired in a 2-D image with the relative delay $t_0$ mapped along the vertical axis, and the wavelength $\lambda$ mapped along the horizontal axis.

Optics EXPRESS

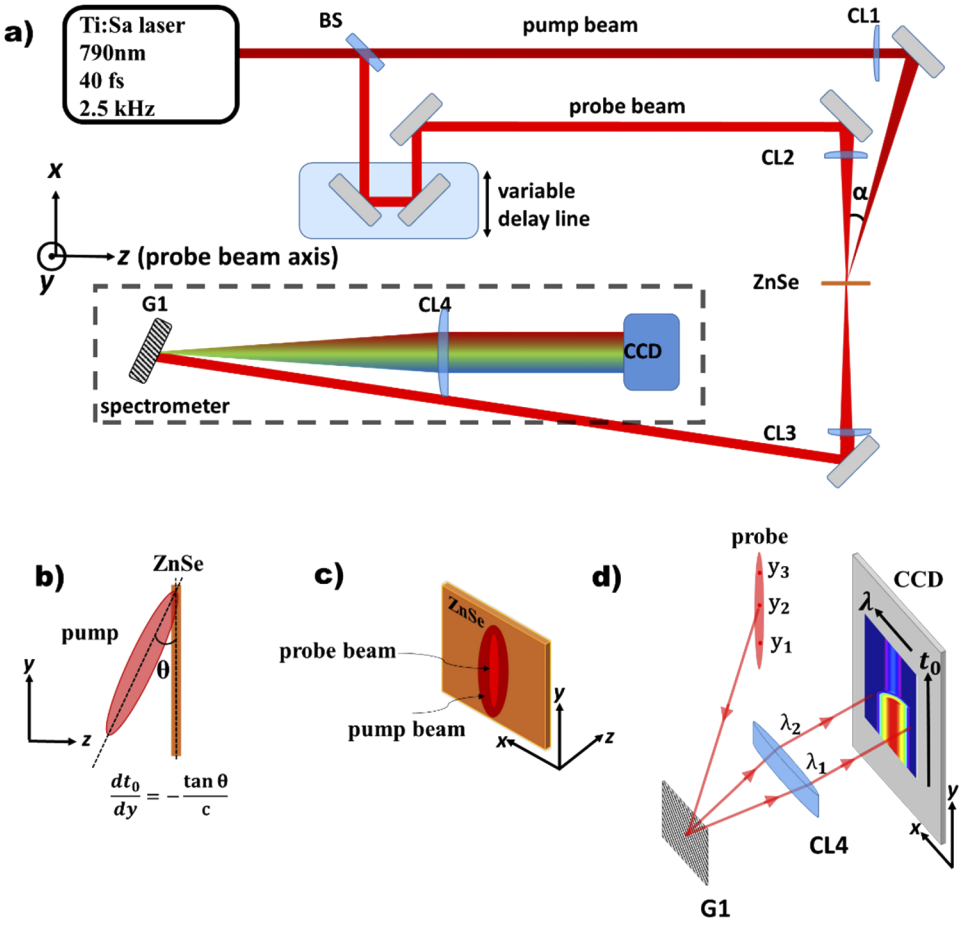


**Fig. 1.** Single-shot acquisition using the FROSt pulse characterization method; a) top-view of the optical layout: BS: beamsplitter; CL1: cylindric lens f=150 mm; CL2:cylindric lens f=80 mm; CL3:cylindric lens f=100 mm; CL4:cylindric lens f=100 mm; G1:grating 600lines/mm; b) Along y, the pump pulse has a delay variation with respect to the surface of the ZnSe sample from the beam incidence angle θ. The upper part of the beam is interacting with the sample earlier than the lower part. c) The probe beam (red) is focused to a sharp vertical line on the surface of the ZnSe sample. The high intensity pump beam (dark red) is also focused to a line covering the probe beam, creating a transient absorption switch as the material is photoexcited. d) Ray tracing showing one position ($y_2$ or delay $t_0(y_2)$) of the probe beam being wavelength resolved in the horizontal dimension after G1 and CL4. Considering all $y$ positions, the resulting 2-D FROSt spectrogram is acquired with a CCD camera to obtain the signal corresponding to the probe spectrum ($x$ direction) as a function of the relative delay between pump/switch and probe ($y$ direction).

Optics EXPRESS

Experimentally, a chirped pulse amplification (CPA) Ti:Sa laser system provides ultrashort pulses at a repetition rate of 2.5 kHz and 790 nm central wavelength with 40 fs duration. In our conditions, the energy of the pump pulse is 120 μJ, corresponding to 300 mW average power measured with a powermeter (UP19 K, Gentec). The energy of the probe pulse is estimated to 0.78 μJ from the Fresnel reflection coefficient of the BS at an incident angle of 45° in p-polarization. The two beams are focused in the $x$ direction at the surface of a 2 mm thick polycrystalline ZnSe sample. The beams remain collimated along the $y$ axis. In the pump arm, the cylindrical lens CL1 focal distance is f = 150 mm and in the probe arm, the cylindrical lens CL2 is f = 80 mm. In this geometry, the beam dimensions are measured by taking images with a CCD camera installed at the ZnSe position where the focused vertical lines overlap. For this, the sample was temporarily removed to measure the beam size and the spatial overlap. The pump beam size is 6.5 mm×75 μm with an estimated Rayleigh range $z_R$~5.5 mm, and the size of the probe beam is 6.5 mm×23 μm, all dimensions at $1/e^2$. Thus, the average fluence of the pump is estimated to 25 mJ/cm$^2$ and that of the probe to 0.05 mJ/cm$^2$. The ZnSe sample is positioned such that its surface matches the intersection plane where the pump and probe beams are overlapping. At this position, the pump fluence is sufficient to create a transient absorption switch that changes rapidly the transmission properties of the material. This mechanism, at the core of the FROSt characterization technique, was reported previously [14,18]. The optical beam path of the pump is adjusted with a translation stage to $t_0(y_2) \sim 0$, so that the switch transition coincides with the center of the probe beam (Fig. 1(d)). Due to incidence angle θ of the pump beam, the relative delay of the switch is continuously varying along the $y$ axis: at vertical position $y_1$, the transition occurs before the arrival of the probe pulse; and at position $y_3$, the transition occurs after. This way, transient absorption spectrograms like illustrated in Fig. 1(d) can be recorded. The horizontal angle α between the pump and probe beams (see Fig. 1(a)) was estimated to 10° in our configuration. This incidence angle is large and makes a non-negligible spatial delay variation of the pump in the direction associated with the wavelength axis of the spectrogram. For example, considering the probe beam size of 23 μm, the pump pulse is sweeping a constant delay range of 13.3 fs in this direction. This effect does not seem to compromise our measurements as long as the acquired spectrogram is encoding a switch $S'(t)$ equivalent to the physical switch $S(t\text{-}t_0)$ integrated over the delay interval associated with the angle α. We are making this assumption as long as $P(t)*S(t\text{-}t_0)$ is a linear operation. To exclude this effect, it is possible to use a beamsplitter or a dichroic mirror to bring the beams parallel in this dimension. After passing through the photo-excited ZnSe sample, the transmitted probe beam is collimated in the $x$ direction with a f=100 mm cylindrical lens (CL3) and is propagated towards a home-built spectrometer made with a 600 l/mm diffraction grating and a second f=100 mm cylindrical lens (CL4), both oriented along the $x$ direction (see Fig. 1(a)). The resulting single-shot FROSt spectrogram is acquired with a CCD camera (Fig. 1(d))).

## 3. Calibration of axes (time and frequency)

The accuracy of this single-shot technique critically depends on the calibration of both transverse axes of the CCD camera acquiring the FROSt spectrograms. This calibration procedure is similar for instance to the calibration of the GRENOUILLE technique [19]. The objective is to determine the delay variation per unit pixel in the vertical direction and the wavelength variation per unit pixel in the horizontal direction. Since both dimensions are orthogonal and decoupled, each dimension requires a different calibration procedure, though in each case the method consists of fitting experimental data points to a linear function that defines the step variation per unit pixel.

First, the delay is calibrated by adding a well-known delay to the optical beam path of the pump pulse by translating a motorized delay stage (Z825B, Thorlabs). This way, the delay variation is known precisely from the relation $\Delta t_0 = 2\Delta z/c$ with $\Delta z$ being the actuator displacement and c the speed of light. In our experiment, we have acquired CCD frame shots for incremental

Optics EXPRESS

displacements of 10 µm, corresponding to individual delay steps of 66.7 fs. In Fig. 2(a), four CCD frame shots are displayed with incremental positions of 10 µm from the reference delay stage.

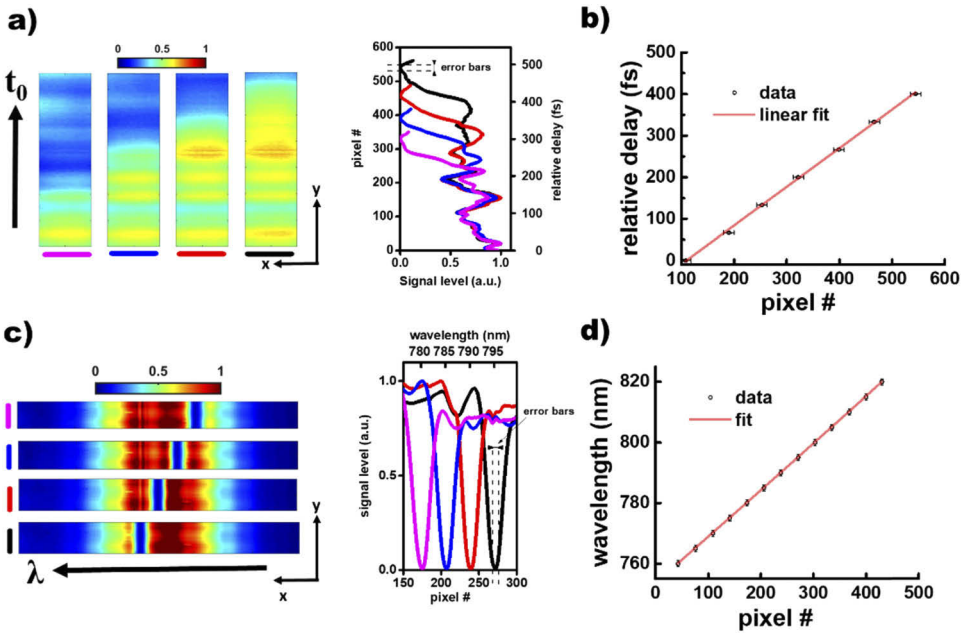


**Fig. 2.** CCD camera axes calibration. a) Frame shots illustrating the calibration procedure for the delay axis. Four single-shot FROSt spectrograms are shown at four different steps of known relative delay between the pump and probe pulses. The frame shot sequence displays the position of the transition moving in the vertical direction. Right panel shows the corresponding integrated profiles (each frame identified with a color line) b) Delay calibration data points and linear fit. c) Frame shots illustrating the calibration procedure of the CCD horizontal axis. A programmable narrowband notch filter is applied to the Ti:Sa laser spectra. It is observed that the hole is changing position as the central wavelength of the notch filter is increased. Right panel shows the corresponding integrated spectrum (each frame identified with color line) d) The spectrogram wavelength calibration is determined from a linear fit of the central wavelength versus pixel position of the hole in the Ti:Sa spectra. For this calibration, the notch filter was varied from 760 nm to 820 nm in steps of 5 nm

The transition of the transmitted signal from high to low intensity in the vertical dimension corresponds to the transient variation of the sample transmissivity resulting from the pump having an incident angle θ in this direction. When the photo-exciting pump comes after the probe, the transmitted signal level is high, and vice-versa. It is observed in each frame that the zero delay position of the switch is moving in the upward direction as the pump delay is increased. In Fig. 2(a), right panel, the normalized integrated profiles showing this transition are displayed. From tracking the pixel position of the minimum, we calibrate the delay axis of the spectrogram. In Fig. 2(b), the linear fit of this switch position versus the applied delay reveals a slope of $0.93 \pm 0.03$ fs/pixel. The calibration error is thus 3.2%, determined from the slope uncertainty provided by the linear fit and mainly originating from small fluctuations in the shape of the absorption profile when the pump delay is varied (see Fig. 2(a), right panel). For this reason, the homogeneity of the photoexcited area is essential to achieve precise calibration since the induced switch must be identical over the delay range, or dimension of interest. In our setup,

Optics EXPRESS

a temporal window of 400 fs corresponds to a separation of 2 mm on the surface of the ZnSe sample where the photo-excitation conditions should be invariable. For single-shot acquisitions, local and small variations of the pump intensity or material properties are also detrimental since the mathematical constraint applied for the spectrogram reconstruction requires *P(t)* and *S(t)* to be global functions.

The spectral axis is calibrated by filtering the Ti:Sa laser spectra with known bandpass filters (programmable notch filter) and correlating the pixel positions along the CCD horizontal position. The notch filters are applied with increments of 5 nm using a programmable filter (Dazzler, Fastlite) installed in the laser frontend [20]. The precise central wavelength of the notch filter is crossed-checked by using an independent spectrometer (USB2000, Ocean Optics), to verify the central wavelength of the holes made in the laser spectra. In Fig. 2(c), four frame shots with different notch filters are presented, showing the hole in the Ti:Sa spectra moving along the wavelength axis as the central wavelength of the filter is increased. The right panel of Fig. 2(c) shows the normalized profiles obtained from the integration of the camera frame shots along the vertical direction. The position of the minima is used for the axis calibration. The axis is calibrated by plotting the pixel positions of the minima with the corresponding central wavelength and applying a second order polynomial fit (see Fig. 2(d)). Using this procedure, we obtained a calibration for the horizontal axis with a dominant linear coefficient of $0.1547 \pm 0.0003$ nm/pixel.

## 4. Results

In order to validate the single-shot implementation of the FROSt technique, two different pulses were measured and the results were compared with standard scanning FROSt measurements acquired in multiple shots employing a motorized translation stage to scan the relative delay between the pump and probe pulses. Such a multiple shot or delay-scanning FROSt setup was described in our previous work [14].

First, the compressed ~40 fs pulses delivered by the CPA laser system are characterized in both configurations with reconstruction results displayed in Fig. 3.

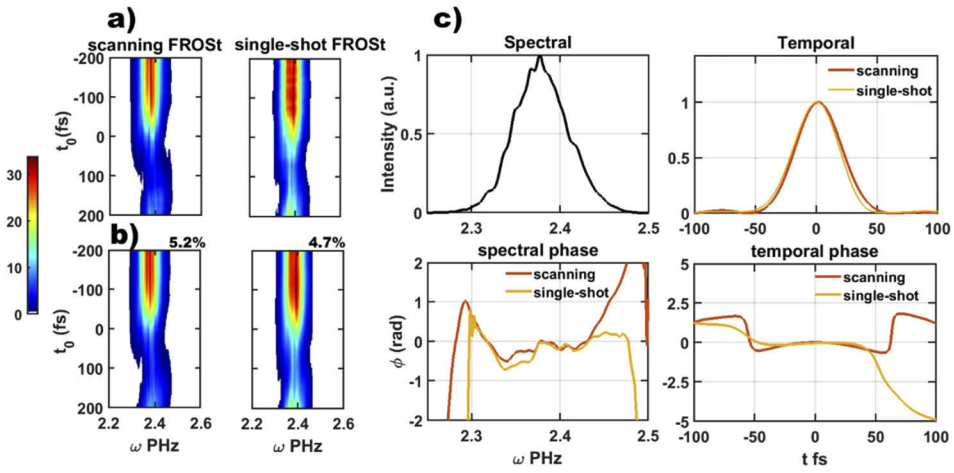


**Fig. 3.** Compressed pulses measured at the laser output. a) Experimental spectrograms acquired in both FROSt configurations. Left panel: delay-scanning FROSt. Right panel: single-shot FROSt. b) Spectrograms obtained after reconstruction. The percentage indicates the reconstruction error, or deviation from the experimental trace. c) Retrieved pulses in amplitude (top panel) and phase (bottom panel) in spectral (left) and time (right) domains. In solid black line, the laser spectrum.

Optics EXPRESS

The acquired and reconstructed spectrograms are displayed respectively in Figs. 3(a) and 3(b), including both FROSt configurations (delay-scanning and single-shot). The laser spectrum has a central wavelength of 790 nm corresponding to angular frequency $\omega_0 = 2.38$ PHz. The reconstruction errors, as defined in the appendix of Ref. [14], are indicated in Fig. 3(b) in percentage and represent the deviation of the experimental traces compared to the traces reconstructed with the retrieved global functions *P(t)* and *S(t)*. The retrieved pulse durations are fairly close for both measurements (Fig. 3(c)) with pulse durations FWHM of 43.0 fs for delay-scanning FROSt and 43.9 fs for single-shot FROSt. However, the pulse duration is not a good accuracy measurement because it does not take into account phase deviations like the one observed in the spectral phase near 2.35 PHz (Fig. 3(c), bottom left). Therefore, we have calculated the root-mean-square field error ε taking values in the interval [0,2] for normalized fields (0 indicating that the two fields are equal and 2 indicating that they are inversions of each other). This accuracy criterion takes into account both the amplitude and phase deviations and is defined as the norm of the field difference [21]. By taking the difference between the fields retrieved in each configuration, we find a value $\varepsilon = 0.18$ which is more representative of the observed discrepancies.

In a second experiment, the pulses are stretched by linear propagation through a highly dispersive material, in this case a 2 mm-thick ZnSe window positioned in the path of the probe pulses. The resulting chirped pulses are characterized in the same manner. The results for the chirped pulses are shown in Fig. 4, with the experimental and reconstructed traces in Figs. 4(a) and 4(b) and the retrieved/measured intensity and phase profiles in Fig. 4(c). The pulse durations FWHM for the stretched pulses are 102 and 109 fs with the delay-scanning FROSt and single-shot FROSt respectively. The root-mean-square error value obtained from the difference of the fields measured in each configuration is $\varepsilon = 0.35$. This higher value is representative of the pulse shape discrepancies observed among the pulses plotted in Fig. 4(c) upper right panel, while the retrieved phases are in good agreement (Fig. 4(c), bottom right panel). In Fig. 4(c), bottom left panel, the phase accumulation in 2 mm ZnSe has been calculated from the Sellmeier equation and has been plotted with the differences obtained from subtracting the phases measured with and without propagation through the 2 mm thick ZnSe window. Then, a fourth order polynomial fit was applied to each curve in order to quantify and compare the measured group-delay dispersion (GDD). The phase has been taken over the spectral bandwidth delimited by the $1/e^4$ level of the peak, in the interval 2.30-2.47 PHz and the fit was developed around the central frequency $\omega_0$=2.38 PHz. This way, the measured GDD values are 1850 $fs^2$ with the delay-scanning FROSt and 2010 $fs^2$ with the single-shot FROSt. In comparison, the value obtained from the Sellmeier equation with 2 mm ZnSe is 2100 $fs^2$.

In Fig. 4(c) right panel, the pulses are plotted along with the numerical propagation of the compressed pulse of Fig. 3 measured in single-shot. The simulated pulse's amplitude and phase resulting from this numerical propagation are displayed in dotted black lines in the right panels of Fig. 3(c). Here also, the pulse amplitude is showing noticeable discrepancies while the phase appears to be in good agreement with the experimental results. The field error value between the pulse propagated numerically and the pulse retrieved in single-shot is $\varepsilon = 0.5$, which is fairly high. We assume that the final pulse shape upon dispersion depends substantially on small variations of the initial phase.

Interestingly, the effect of the switch observed in both FROSt configurations are quite different but the pulses can still be retrieved. Since the pump pulse was the same in each configuration, we attribute the difference in the transient response for each setup to the lower fluence applied at the surface of the material in single-shot. In this case, the pump beam was spread over a larger area for the spatial encoding of the delay axis and the fluence was thus limited to 25 $mJ/cm^2$. The transient response can be observed in Fig. 4(a): for the single-shot FROSt trace, the signal drops by more than 60% just after the transition and then increases rapidly as the material transmissivity

Optics EXPRESS

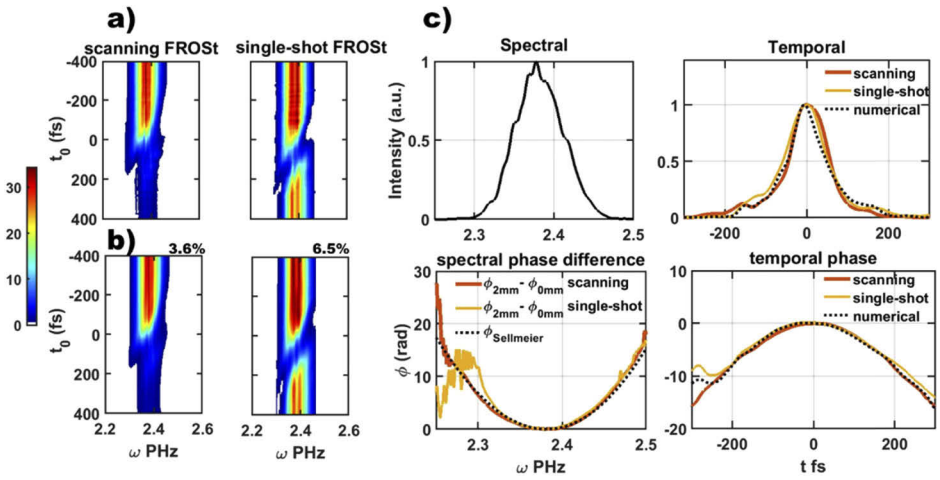


**Fig. 4.** Characterization of pulses stretched after propagation through dispersive material. a) Experimental spectrograms acquired with both FROSt configurations. Left panel: delay-scanning FROSt. Right panel: single-shot FROSt. b) Spectrograms obtained after reconstruction. The percentage indicates the reconstruction error. c) Retrieved pulses in amplitude (top right panel) and phase (bottom right panel). In solid black line, the laser spectrum (top left panel). The spectral phase difference plot (bottom left) is displaying the difference of the phases measured with and without the dispersive material (2 mm ZnSe). The phase in dotted black line represents 2 mm ZnSe propagation calculated from the Sellmeier equation. In temporal domain (right panels), the pulse retrieved in Fig. 3 is propagated numerically and the resulting amplitude and phase are displayed in dotted black lines.

recovers to reach a remaining drop of about only 20%. In comparison, for the scanning FROSt trace, the signal remains low after the transition and no relaxation of the photoexcited material occurs in this delay range. In that latter case, the fluence was not limited and the pump energy was adjusted to obtain a remaining drop of transmissivity of almost 90%. Nevertheless, the pulse in amplitude and phase *P(t)* is retrieved independently of *S(t)*. However, pumping the material at low fluence level, in combination with a photon energy below the material's bandgap is not advised. In these conditions, there is a possibility, although it was not verified here, that the switch is generated below the surface of the material since the pump photon energy (1.55 eV) is below the bandgap of ZnSe (2.70 eV). If so, the propagation of the pulse *P(t)* before interacting with the switch *S(t)* would affect the measurements. Typically, we choose a pump with photon energy above bandgap so that the absorption is linear and the penetration depth near the surface, up to a few microns. This aspect was discussed in our previous publication [14].

## 5. Conclusion & outlook

In this paper, we have demonstrated a basic implementation of the FROSt method for single-shot pulse characterization. We have successfully characterized pulses delivered from a standard Ti:Sa CPA laser system. In the perspective of developing an instrument with increased robustness and reliability, the setup could be further improved by including a more sophisticated imaging spectrometer built with a vertical slit at the entrance like a Czerny-Turner design [22]. The probe beam interacting at the surface of the material could be imaged directly at the entrance slit of such a spectrometer and the 2-D FROSt image acquired directly at the exit plane. In the future, single-shot implementation of the FROSt technique could be useful especially for ultra-broadband and low repetition rate laser systems in the visible or near-infrared spectral range

Optics EXPRESS

[13]. Even infrared and mid-infrared single-shot FROSt measurements are possible with a 2-D array detector in the required wavelength range.

## Disclosures

The authors declare no conflicts of interest.

## References


1. R. Trebino, *Frequency-resolved optical gating: the measurement of ultrashort laser pulses* (Springer Science & Business Media, 2012).
2. I. A. Walmsley and C. Dorrer, "Characterization of ultrashort electromagnetic pulses," Adv. Opt. Photonics **1**(2), 308–437 (2009).
3. C. Iaconis and I. A. Walmsley, "Self-referencing spectral interferometry for measuring ultrashort optical pulses," IEEE J. Quantum Electron. **35**(4), 501–509 (1999).
4. T. Oksenhendler, S. Coudreau, N. Forget, V. Crozatier, S. Grabielle, R. Herzog, O. Gobert, and D. Kaplan, "Self-referenced spectral interferometry," Appl. Phys. B **99**(1-2), 7–12 (2010).
5. D. J. Kane and R. Trebino, "Single-shot measurement of the intensity and phase of an arbitrary ultrashort pulse by using frequency-resolved optical gating," Opt. Lett. **18**(10), 823–825 (1993).
6. P. O'Shea, M. Kimmel, X. Gu, and R. Trebino, "Highly simplified device for ultrashort-pulse measurement," Opt. Lett. **26**(12), 932–934 (2001).
7. T. Nagy and P. Simon, "Single-shot TG FROG for the characterization of ultrashort DUV pulses," Opt. Express **17**(10), 8144–8151 (2009).
8. J. Shan, A. S. Weling, E. Knoesel, L. Bartels, M. Bonn, A. Nahata, G. A. Reider, and T. F. Heinz, "Single-shot measurement of terahertz electromagnetic pulses by use of electro-optic sampling," Opt. Lett. **25**(6), 426–428 (2000).
9. D. Fabris, W. Holgado, F. Silva, T. Witting, J. W. G. Tisch, and H. Crespo, "Single-shot implementation of dispersion-scan for the characterization of ultrashort laser pulses," Opt. Express **23**(25), 32803–32808 (2015).
10. L. Yu, X. Liang, J. Li, A. Wu, Y. Zheng, X. Lu, C. Wang, Y. Leng, J. Xu, and R. Li, "Experimental demonstration of joule-level non-collinear optical parametric chirped-pulse amplification in yttrium calcium oxyborate," Opt. Lett. **37**(10), 1712–1714 (2012).
11. V. Ginzburg, I. Yakovlev, A. Zuev, A. Korobeynikova, A. Kochetkov, A. Kuzmin, S. Mironov, A. Shaykin, I. Shaikin, E. Khazanov, and G. Mourou, "Fivefold compression of 250-TW laser pulses," Phys. Rev. A **101**(1), 013829 (2020).
12. E. A. Anashkina, V. N. Ginzburg, A. A. Kochetkov, I. V. Yakovlev, A. V. Kim, and E. A. Khazanov, "Single-shot laser pulse reconstruction based on self-phase modulated spectra measurements," Sci. Rep. **6**(1), 33749 (2016).
13. S. Y. Mironov, S. Fourmaux, P. Lassonde, V. N. Ginzburg, S. Payeur, J.-C. Kieffer, E. A. Khazanov, and G. Mourou, "Thin plate compression of a sub-petawatt Ti:Sa laser pulses," Appl. Phys. Lett. **116**(24), 241101 (2020).
14. A. Leblanc, P. Lassonde, S. Petit, J. C. Delagnes, E. Haddad, G. Ernotte, M. R. Bionta, V. Gruson, B. E. Schmidt, H. Ibrahim, E. Cormier, and F. Légaré, "Phase-matching-free pulse retrieval based on transient absorption in solids," Opt. Express **27**(20), 28998–29015 (2019).
15. A. Leblanc, G. Dalla-Barba, P. Lassonde, A. Laramée, B. E. Schmidt, E. Cormier, H. Ibrahim, and F. Légaré, "High-field mid-infrared pulses derived from frequency domain optical parametric amplification," Opt. Lett. **45**(8), 2267–2270 (2020).
16. P. Sidorenko, O. Lahav, Z. Avnat, and O. Cohen, "Ptychographic reconstruction algorithm for frequency-resolved optical gating: super-resolution and supreme robustness," Optica **3**(12), 1320–1330 (2016).
17. A. Brun, P. Georges, G. L. Saux, and F. Salin, "Single-shot characterization of ultrashort light pulses," J. Phys. D: Appl. Phys. **24**(8), 1225–1233 (1991).
18. F. Cilento, C. Giannetti, G. Ferrini, S. D. Conte, T. Sala, G. Coslovich, M. Rini, A. Cavalleri, and F. Parmigiani, "Ultrafast insulator-to-metal phase transition as a switch to measure the spectrogram of a supercontinuum light pulse," Appl. Phys. Lett. **96**(2), 021102 (2010).
19. B.-K. Yang, H. Seok Rho, J. Myung Seo, and J. Seung Kim, *Design, Construction and Calibration of a GRENOUILLE, Single-Shot, Ultrashort-Pulse Measurement System* (2008), Vol. 52.
20. P. Tournois, "Acousto-optic programmable dispersive filter for adaptive compensation of group delay time dispersion in laser systems," Opt. Commun. **140**(4-6), 245–249 (1997).
21. C. Dorrer and I. A. Walmsley, "Accuracy criterion for ultrashort pulse characterization techniques: application to spectral phase interferometry for direct electric field reconstruction," J. Opt. Soc. Am. B **19**(5), 1019–1029 (2002).
22. D. R. Austin, T. Witting, and I. A. Walmsley, "Broadband astigmatism-free Czerny-Turner imaging spectrometer using spherical mirrors," Appl. Opt. **48**(19), 3846–3853 (2009).